ERCOFTAC
Classic Collection Database

# COMBINED FLOW AND DEFORMATION MEASUREMENTS OF FSI-INDUCED OSCILLATION OF A BLUFF FLEXIBLE STRUCTURE IN UNIFORM FLOWS

*in section* Flows Around Bodies / Two-dimensional flows / 7. Around oscillating bodies or with unsteady approach flow

Author(s):
**JORGE PEREIRA GOMES and HERMANN LIENHART**
2011 • EXPERIMENTAL

Institute of Fluid Mechanics and
Erlangen Graduate School in Advanced Optical Technologies,
University of Erlangen-Nuremberg,
Cauerstrasse 4, D-91058 Germany
jgomes@lstm.uni-erlangen.de / lienhart@lstm.uni-erlangen.de

# 1. Description

Characterisation of the FSI-induced two-dimensional limit-cycle oscillation (LCO) of a flexible structure consisting of a bluff front end in uniform flows. The measurements were performed for different fluid viscosities and approaching flow velocities and covered both laminar and turbulent flow regimes. At the total, 2 test cases were measured in laminar and 1 test case in turbulent flows. The measurements in the turbulent regime were conducted in water whereas a highly viscous polyethylene glycol (PEG) syrup was chosen as test liquid for the tests in laminar flows.

# 2. Geometrical parameters

## 2.1 Model definition

The structure model is presented in figure 2.1. It consists consisted of a *0,04* mm thick stainless-steel sheet attached to a free rotating *22* mm diameter circular cylinder. At the trailing edge of the thin sheet, a rectangular mass was considered. The overall length of the model was defined as *82* mm and the spanwise dimension was chosen to be equal to the spanwise dimension of the test section to guarantee the two-dimensionality of the experiments. Just a small gap of *1,5* mm between the model and the walls of the test section was set in order to avoid any possible friction between the moving parts of the model and the walls.
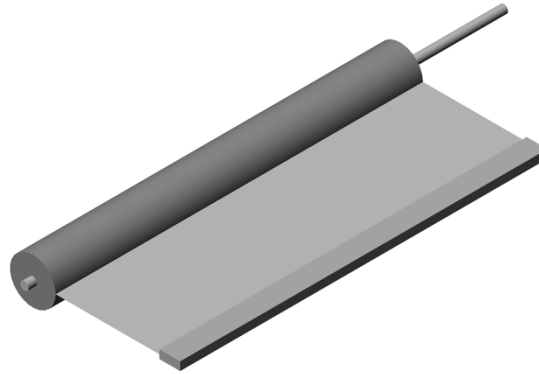


*Figure 2.1 – Flexible structure model.*

The geometric definition of the model is presented in figure 2.2. Table 2.1 summarizes the mechanical and dynamic properties of this model.
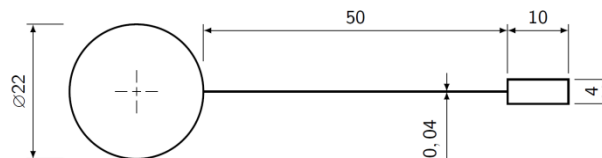


*Figure 2.2 – Geometry of the flexible structure model (dimensions in mm).*

| | |
|---|---|
| $\rho_{front\ body}$ [kg/m$^3$] | 2828 |
| $E_{thin\ sheet}$ [kN/mm$^2$] | 200 |
| $\rho_{thin\ sheet}$ [kg/m$^3$] | 7855 |
| $\rho_{rearmass}$ [kg/m$^3$] | 7800 |
| $m$ [g] | 248,8 |
| $I_0$ [kg m$^2$] | 2,59E-4 |
| $x_{CM}$ [mm] | 15,20 |
| $f_0$ [Hz] | 1,90 |
| $f_1$ [Hz] | 5,89 |
| $f_2$ [Hz] | 27,43 |
| $f_3$ [Hz] | 92,73 |

*Table 2.1 – Property values of the flexible structure model.*

The measurements were conducted in a vertical, closed-loop tunnel capable of operating with liquids of different viscosities. The spatial dimensions of the tunnel test section are presented in figure 2.3. It had a *180* mm × *240* mm cross-sectional area and a total length of *380* mm. As a direct consequence of the vertical orientation of the tunnel, the gravity force was aligned with the flow (*x*-axis, see figure 2.3). In this way, the gravity force did not introduce any asymmetry in the experiments. All test models were mounted *55* mm downstream of the inlet plane of the test section with a free rotational degree-of-freedom. The supporting system used two low friction bearings and was designed to guarantee frictionless rotation of the model around the *z*-axis (see figure 2.3).
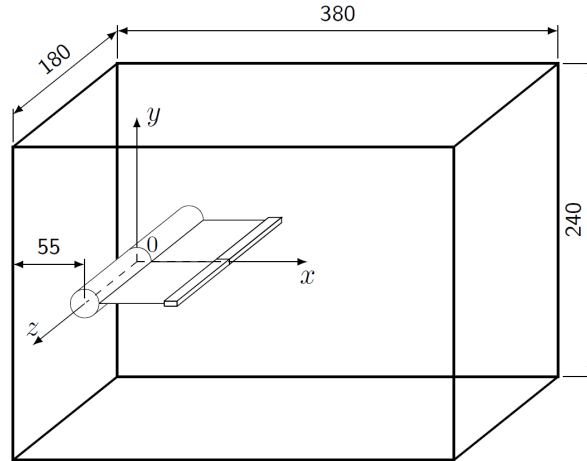


*Figure 2.3 – Test section geometry (dimensions in mm).*

## 3. Flow parameters

The fluid properties for the different test cases are summarized in table 3.1. Within the temperature range of the tests, the kinematic viscosity and density of the fluid were measured to be constant.

| Test case | $U_\infty$ [m/s] | Re[a] [-] | $\nu$ [m²/s] | $\rho$ [kg/m³] |
|---|---|---|---|---|
| LL1 | *1,07* | *145* | *1,64E-4* | *1050* |
| LL2 | *1,45* | *195* | *1,64E-4* | *1050* |
| TL1 | *0,68* | *15400* | *0, 97E-6* | *998* |

[a] based on the diameter of the front body of the model.

*Table 3.1 – Flow parameters.*

The test cases inlet velocity conditions were characterized in the absence of any model at the location *x = -55* mm in the centre plane of the test section (*z=0* mm, see figure 2.3). The flow angularity was measured to be less than *0,5°* and the RMS value associated with the fluctuation of the magnitude of the velocity was less that *1%*. These values, and also the mean flow velocity, corresponded to the interval *-85* mm $\leq y \leq 85$ mm.

The inlet velocity profile is available for each test case in the following files:

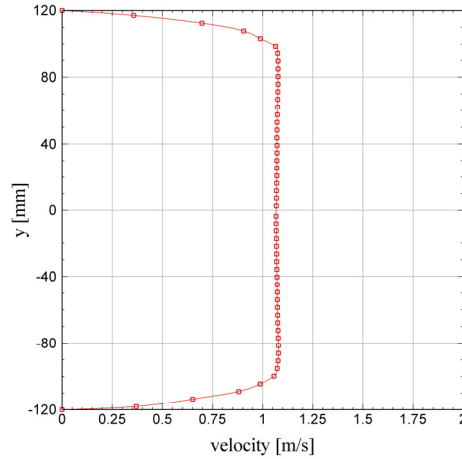| test case | file name | quantities |
|---|---|---|
| LL1 ($U_\infty = 1,07$ m/s) | LL1_Inlet_Velocity_Profile.txt | $U_\infty(y)$ |
| LL2 ($U_\infty = 1,45$ m/s) | LL2_Inlet_Velocity_Profile.txt | $U_\infty(y)$ |
| TL1 ($U_\infty = 0,68$ m/s) | TL1_Inlet_Velocity_Profile.txt | $U_\infty(y)$ |

Example:



*Figure 3.1 – File LL1_Inlet_Velocity_Profile.txt.*


## 4. Experimental details

### 4.1 Flow field measurements

The flow velocity field was measured using a DANTEC two-dimensional, two-component particle image velocimetry (PIV) system. For the acquisition of the images, two synchronized *1280* pixel × *1024* pixel CCD cameras equipped with *60* mm focal length macro lenses were adopted to acquire two simultaneous and adjacent time-dependent pairs of images from the centre plane of the test section (*xy*-plane, see figure 2.3). The PIV images acquired by the two cameras were then imported into a MatLab-based post-processing script to stitch the corresponding pairs of images before being correlated. Opting for this solution, it was possible to achieve an extended *270* mm × *170* mm flow field measuring area while keeping the spatial resolution of the measurements as high as *7,53* CCD pixel/mm.

For the ilumination of the flow, two laser light sources were used from both sides of the test section, each to illuminate the flow at each side of the model, and, therefore, to avoid any shadow region in the flow. The lasers were of the double-head pulsed Nd:YAG type and delivered light pulses of a wavelength of *532* nm with a maximum energy of *120* mJ.

As seeding particles, *10* μm mean diameter hollow glass spheres were chosen. Non-coated spheres were used for the test case TL1 whereas silver-coated spheres were used for test cases LL1 amd LL2.


### 4.2 Structure deformation measurements

To measure the position of the structure, a stereo pattern recognition (SPR) measuring system was adopted. Two synchronized cameras were mounted in a stereoscopic arrangement to acquire images of the flexible structure illuminated by a laser light sheet from each side of the model. The quantitative analysis was performed after the images acquisition in the MatLab workspace by a script developed for the specific task. The software analysed and compared the images from both sides of the model and reconstructed to scale the image of the light sheet reflected by the structure. To achieve that propose, it mapped the pixel value in the gray-scale of the entire image and detected the line resulting from the intersection of the laser sheet and the structure. The recognition of the reflection line, and posterior reconstruction of the structure deformation, was performed in the mathematical space, based on calibrated reference images.


### 4.3 Reconstruction of the measurements in the time-phase space

The measuring system was operated at constant acquisition rate and the reconstruction of the measurements in the time-phase space was performed during the post-processing period. This approach was chosen instead of triggering the data acquisition by the experiment in order to coupe with the usual cycle-to-cycle fluctuation of the structure oscillation period found in free oscillation tests. Figure 4.1 shows a typical data reconstruction using this method. Simultaneously with the acquisition of the measurements, two kind of events, the acquisition of the measurements $tm_i$ [figure 4.1(B)] and the beginning of the movement cycles $tc_j$ [figure 4.1(A)], were recorded. These time events were detected using the camera trigger signal and the signal of an angular position sensor located in the rotating axle of the structure, respectively.
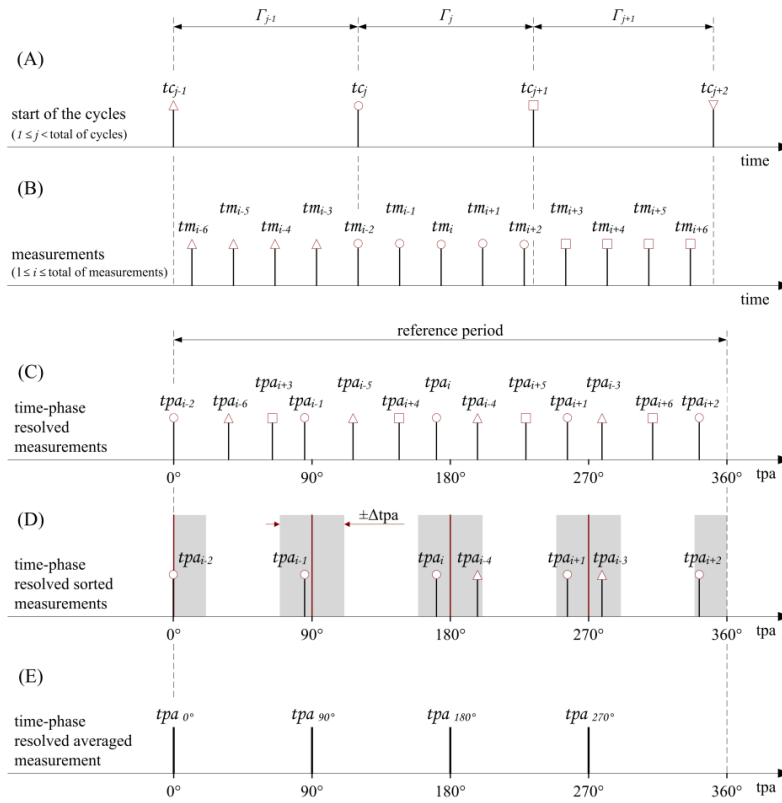
*Figure 4.1 – Time-phase resolved measurements reconstruction scheme.*

The event monitoring was performed by an hardware module designed based on a field programmable gate array (FPGA) and a *1* MHz internal clock. It was capable to record up to *250* events per second with an accuracy of *2* μs.

From the recorded events time information, a post-processing software computed the time-phase angle $\varphi$ for each acquired measurement. At this point, the resolved measured data could be reorganized in a reference period $\bar{\Gamma}_j$ equal to the mean period of all acquired cycles [figure 4.1(C)] to be sorted out according to a predefined time-phase angle resolution and uncertainty [figure 4.1(D)]. Finally, the data falling within one time-phase angle slot were averaged to obtain the final result [figure 4.1(E)]. In the present test cases, the reconstruction of the experimental results was performed with a time-phase resolution and uncertainty of *5°* and *0,5°*, respectively, and the final result corresponded to the mean value of *100* realizations.

## 5. Experimental data

All data corresponding to the present test cases can be downloaded as a single file as follows:

| L_Data_All_Files.rar |
| --- |
| L_Data_All_Files.gz |
| L_Data_All_Files.7z |

All experimental results are organized in the test cases. Table 5.1 shows the frequency of the limit cycle oscillation of the model together with the RMS value associated with the cycle-to-cycle fluctuation registered during the data acquisition.

| | |
| --- | --- |
| LL1 ($U_\infty = 1,07$ m/s) | *6,38* Hz $\pm 0,6$ % |
| LL2 ($U_\infty = 1,45$ m/s) | *13,58* Hz $\pm 0,9$ % |
| TL1 ($U_\infty = 0,68$ m/s) | *4,45* Hz $\pm 0.4$ % |

*Table 5.1 – Oscillation frequency of the model.*

The time-phase trace of the angle of the model front body ($\theta$) within an oscillation period is available in the following files:

| test case | file name | quantities |
|---|---|---|
| LL1 ($U_\infty = 1,07$ m/s) | LL1_Front_Body_Angle.txt | $\theta(\varphi)$ |
| LL2 ($U_\infty = 1,45$ m/s) | LL2_Front_Body_Angle.txt | $\theta(\varphi)$ |
| TL1 ($U_\infty = 0,68$ m/s) | TL1_Front_body_Angle.txt | $\theta(\varphi)$ |

The successive positions of the model trailing edge ($x_{TE}$; $y_{TE}$) within an oscillation period is available in the following files:

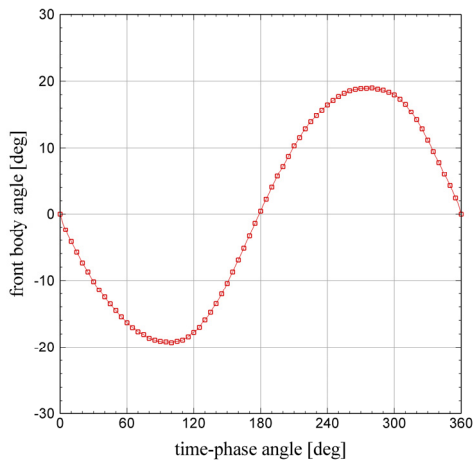| test case | file name | quantities |
|---|---|---|
| LL1 ($U_\infty = 1,07$ m/s) | LL1_Trailing_Edge_Coordinates.txt | $x_{TE}(\varphi)$ ; $y_{TE}(\varphi)$ |
| LL2 ($U_\infty = 1,45$ m/s) | LL2_Trailing_Edge_Coordinates.txt | $x_{TE}(\varphi)$ ; $y_{TE}(\varphi)$ |
| TL1 ($U_\infty = 0,68$ m/s) | TL1_Trailing_Edge_Coordinates.txt | $x_{TE}(\varphi)$ ; $y_{TE}(\varphi)$ |

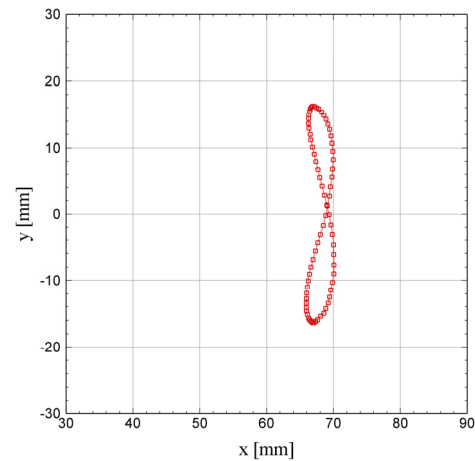Examples:



*Figure 5.1 – File LL1_Front_Body_Angle.txt.*

*Figure 5.2 – File LL1_Trailing_Edge_Coordinates.txt.*

The time-phase resolved data on the flow velocity field and model deformation is available in the following packages:

| test case | file name | quantities |
|---|---|---|
| LL1 ($U_\infty = 1,07$ m/s) | LL1_tpa_Files.rar | $\theta(\varphi)$ ; $x_{TE}(\varphi)$ ; $y_{TE}(\varphi)$ ; $x(\varphi)$ ; $y(\varphi)$ $u(\varphi;x;y)$ ; $v(\varphi;x;y)$ ; $(u^2+v^2)^{1/2}(\varphi;x;y)$ |
| LL2 ($U_\infty = 1,45$ m/s) | LL2_tpa_Files.rar | $\theta(\varphi)$ ; $x_{TE}(\varphi)$ ; $y_{TE}(\varphi)$ ; $x(\varphi)$ ; $y(\varphi)$ $u(\varphi;x;y)$ ; $v(\varphi;x;y)$ ; $(u^2+v^2)^{1/2}(\varphi;x;y)$ |
| TL1 ($U_\infty = 0,68$ m/s) | TL1_tpa_Files.rar | $\theta(\varphi)$ ; $x_{TE}(\varphi)$ ; $y_{TE}(\varphi)$ ; $x(\varphi)$ ; $y(\varphi)$ $u(\varphi;x;y)$ ; $v(\varphi;x;y)$ ; $(u^2+v^2)^{1/2}(\varphi;x;y)$ |

Each package contains *72* files correspondent to different time-phase angles within an oscillation period. The experimental results obtained at the beginning of the oscillation period ($\varphi=0°$) are stored in the file _0000.txt, and the final measuring point corresponded to $\varphi=355°$ and the results are stored in the file named _3550.txt. The intermediate measuring points were defined with a time-phase resolution of *5°* and the results for $\varphi=360°$ are identical to those

for $\varphi=0°$. The files also considered a prefix which identifies the test case the files belong. For example, file *LL1_0450.txt* corresponds to the first test case (LL1, $U_\infty$ = *1,07* m/s) and contains the results obtained for the time-phase angle $\varphi=45°$.

All files have a similar structure which is explained in figure 5.6 (using the file *LL1_0450.txt* as an example). About the flow velocity field results, the measuring location was set to the middle plane of the experimental domain (*z=0*, see figure 2.3) and considered a *270* mm × *170* mm rectangular measuring area. The area, which extended from −*35* mm up to *235* mm in the *x*-direction and from −*85* mm up to *85* mm in the *y*-direction, is represented in figure 5.3.
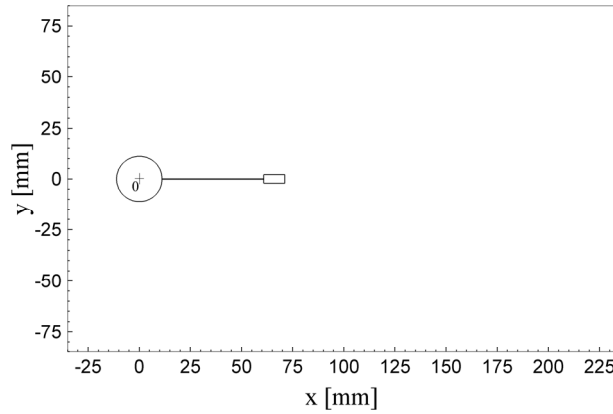


*Figure 5.3 –Measuring area.*

The spatial resolution of the velocity field measurements was defined as *2,1* mm and the accuracy associated with them was measured better than *1,5%* for the undisturbed flow. Both the *u-* and *v*-components and also the magnitude of the velocity were normalized by the free stream flow velocity, $U_\infty$.

As far as the model deformation is concerned, the results compreend just the flexible part of the model. That corresponds to the points between *x=11* mm and *x=61* mm (*y=0* mm) of the undeformed model (see figure 5.3). The position of the rear mass is given by the deformed position of the last point of the flexible part of the model and the position of the model trailing edge. The RMS value associated with the fluctuation of the structure deformation results was evaluated as *0,26* mm for test cases LL1 and LL2 and *0,4* mm for the test case TL1, within an interval of confidence of *90%*.
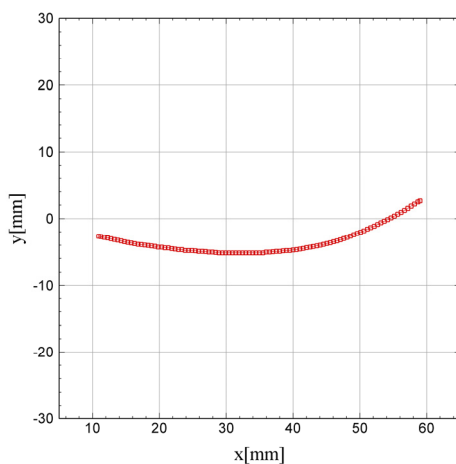
Examples:



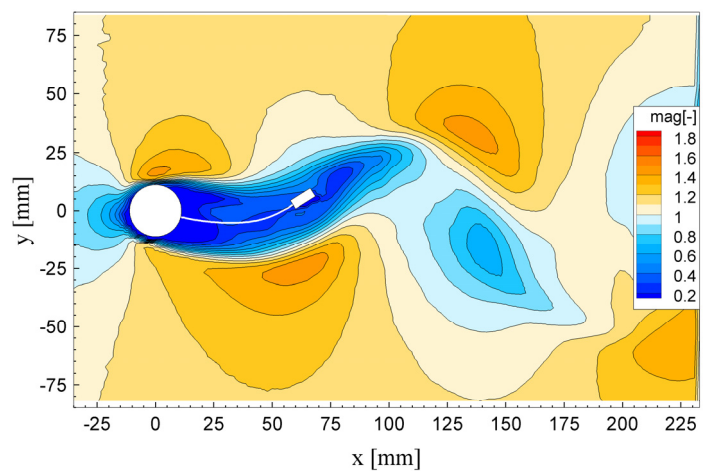*Figure 5.4 –Model deformation results from file LL1_0450.txt.*



*Figure 5.5 – Flow velocity magnitude results from file LL1_0450.txt.*

```
Test:
LL1                                 --------   test case to which the measurements correspond

Time-phase angle (deg):
45.0                                --------   time-phase angle to which the file corresponds (φ in deg)
Number of measurements (-):
137                                 --------   number of measurements used in the averaging of the results

Inlet velocity (m/s):
1.07                                --------   inlet flow velocity (U∞ in m/s)

Frequency of the motion: (Hz):
6.38                                --------   oscillation frequency of the model (f in Hz)
Front body angle of attack (deg):
-13.55                              --------   angle of the model front body (θ in deg)
Trailing edge coordinates:
x(mm)   y(mm)
67.36   7.97                        --------   coordinates of the trailing edge of the model (xTE, yTE in mm)

Structure deflection:
#97                                 --------   number of points in the model deformation(*)
x(mm)   y(mm)
10.93   -2.65       ⎫
11.25   -2.71       ⎪
...                 ⎬              coordinates of the deformed position of the model (x, y in mm)
58.69   2.49        ⎪              [number of lines given in (*)]
59.00   2.65        ⎭

Velocity field
#10112                              --------   number of measuring points in the flow field(**)
x(mm)   y(mm)   u(-)  v(-)  magnitude(-)
235.002 -82.126 0.000  0.000  0.000    ⎫
232.876 -82.126 1.262  0.016  1.262    ⎬   flow velocity field (x, y in mm; u, v, velocity magnitude
...                                    ⎪   normalised by U∞)
-32.963  83.769 1.088  0.004  1.088    ⎪   [number of lines given in (**)]
-35.090  83.769 1.084 -0.005  1.084    ⎭
```

*Figure 5.6 – File  LL1_0450.txt.*

## Acknowledgements

## References

[1] Gomes, J. P. (2011) *Fluid-structure interaction-induced oscillation of flexible structures in uniform flows*, Ph.D. Thesis.

[2] Gomes, J. P. and Lienhart, H. (2009) Experimental Benchmark: Self-excited Fluid-structure Interaction Test Cases, in *Fluid-Structure Interaction II: Modelling, Simulation, Optimisation*, Bungartz, H. J., Mehl, M., Schäfer, M. (eds.), **383-412**, Springer-Verlag.

[3] Gomes, J. P., yigit, S., Lienhart, H., Schäfer, M. (2011) Experimental and Numerical Study on a Fluid-structure Interaction Reference Test Case, *Journal of Fluids and Structures*, **27**, 43-61.